

LAGRANGIAN PARTICLE TRACKING POST-PROCESSING FOR LINKING CFD TO BIOREACTOR ANALYSIS

Petar LIOVIC^{1*}, Ilija D. ŠUTALO^{2*} and Joseph D. BERRY^{3*}

¹ CSIRO Minerals Resources, Clayton, Victoria 3169, AUSTRALIA

² Department of Chemistry, Monash University, Victoria 3800, AUSTRALIA

³ Department of Chemical and Biomolecular Engineering, University of Melbourne, Victoria 3010, AUSTRALIA

*Corresponding author, E-mail address: Petar.Liovic@csiro.au

ABSTRACT

A Lagrangian particle tracking (LPT) solver is presented that can be used for studying culture, cell and particle interactions in flows, through coupling of the LPT solver to the Computational Fluid Dynamics (CFD) in post-processing. The LPT solver is part of a three-way coupling strategy for flows dilutely laden with particles but in which particle-particle interactions are potentially important. The LPT solver is used as a post-processor, in conjunction with a strategy for mapping fluid flow data from the relevant historical fluid-only CFD database to Lagrangian particle locations. This strategy is effective in enabling cell-fluid, cell-particle and cell-cell interactions in stirred-tank bioreactor (STR) flows to be studied without requiring repeated CFD computations. In particular, studies of bioreactor STR particle inclusions can be iterated rapidly using historical CFD data sets using this approach, rather than repeated coupled CFD/LPT simulations for any change in inclusions. The LPT solver is used to reveal density effects on particle suspension and stress exposures.

NOMENCLATURE

t	time
m_p	particle mass
I_p	particle moment of inertia
\mathbf{U}_p	particle (translational) velocity
ω_p	particle angular velocity
\mathbf{F}_p	total force acting on particle
\mathbf{T}_p	total torque acting on particle
ρ_p	particle density

INTRODUCTION

Extension of stirred-tank bioreactor (STR) usage from mammalian and microbial culture fermentation to stem cell expansion has been inspired in recent years by the research efforts of STR manufacturers that have been documented as technical notes. Examples such as Eppendorf STRs (Olmer et al. (2013)) and Millipore STRs (2013) provide confidence that rapid stem cell expansion can be achieved. Of course outcomes reported in such technical notes are specific to the culture studied, and deviations in the culture conditions associated with the development of new cultures cast doubt on expectations

that many-fold expansions reported in such technical notes will be achieved.

For a culture strategy based on the use of microcarriers, many changes in culture and operational protocols can be conceived that can result in underperformance of the stem cell bioreactor. A typical change in a STR for stem cell expansion using microcarrier particles is a change in particle type. For example, a lighter particle is expected to suspend easier upon commencement of agitation in the STR, but is also expected to settle slower. On the one hand, better microcarrier suspension is expected to increase the number of microcarriers exposed to potential contact with stem cells and the rate of cell/microcarrier collisions. On the other hand, slower settling reduces the frequency of spin-up cycles in operating protocols, hence reduces the time window over which collisions between cells and suspended microcarriers can occur, and also reduces the turnover of microcarriers on top of the packed bed in the settled period of an operational protocol during which collisions between settled and settling cells and microcarriers occur.

More generally, the function and behaviour of cells is governed by cell-local chemomechanical microenvironments that are ever changing. This makes STR stem cell bioreactor performance not just a function of the collisions involved, and perhaps not even primarily so. Additionally, the trajectories of the cells in culture are important because of alternative and coupled chemical and mechanical effects that can affect cell expansion, viability and lineage potential. In the case of the chemical microenvironment, cell signalling involving signalling proteins will play a role, although controlling exposure to such cell signals is more difficult than if other forms of stem cell bioreactors are used (such as those considered in Berry et al. (2015)). In STRs, the usual aspects of the chemical environment that tend to be monitored include standard conditions, such as dissolved oxygen, carbon dioxide and pH. The feature of the mechanical microenvironment that affects stem cells is shear stress exposure, with very high stresses able to cause cell damage and reduce cell viability (Croughan et al. 1987), and moderately high stresses able to impact on lineage potential (e.g. Zhao et al. 2007; Park et al. 2010). These mechanical effects are also influenced by the chemical environment.

Computational Fluid Dynamics (CFD) has made valued inroads into the study of stirred tank bioreactors (including works by the current authors). It is worth noting, however, that microcarriers and stem cells in the CFD of stem cell bioreactors represent disproportionately large modelling challenges that make the utility of CFD to projects developing stem cell bioreactor technologies marginal. The cost of adequately tooled CFD for investigating stem-cell bioreactors (fully coupling the culture fluid flow with particle interactions associated with microcarriers and with cells) is relatively substantial, and indeed raises the prospect of physical experiments being affordable (relative to CFD). In the context of CFD capability competing with experimentalists for funding from projects, a framework for reducing the computational effort in full-reactor studies through reduced coupling between the fluid flow and the particle solutions is potentially valuable. Investigating different particle system properties using the results of only one CFD computation is a significant cost saving in itself, and enables longer-duration simulations to allow longer time-scale biological processes associated with stem cell bioreactor operations to be studied.

In this paper, a nimble Lagrangian particle tracking (LPT) solver is presented that can be used for studying cell-fluid, cell-particle and cell-cell interactions in STR flows, through coupling of the LPT solver to the CFD via post-processing of fluid-only historical CFD results databases. This paper presents the LPT solver and investigates some of the potential limitations associated with the reduced coupling between the particle and fluid flow solutions, before demonstrating the utility of the LPT post-processor as a component of a virtual environment for bioreactor analysis.

MODEL DESCRIPTION

The model consists of a Lagrangian particle tracking solver that reads in fluid flow data from a relevant database of results from a previous fluid-only CFD simulation. The CFD computation is first briefly discussed, before the LPT solver is presented. The mapping of data from the CFD database to the LPT solver is then discussed, before additional issues relating to temporal fluctuations in the fluid flow not resolved in the CFD database are discussed.

Stirred-tank bioreactor bath: CFD computation

The STR flow considered in the current work is that within a 3L Millipore Mobius single-use STR filled with 2.2 L of water. A marine impeller operating at 90 RPM low down in the STR achieves impeller-based agitation of the liquid bath. In the current study, there is no gas-sparging contribution to the agitation, with gas exchange only occurring across the free surface. At 90 RPM, the marine impeller achieves strong mixing lower down in the bath, but this reduces going up in the bath, to the extent that the free surface remains relatively flat during the course of fully developed STR operation. As a result, the fluid flow model reduces to single-fluid CFD, which enables the relatively uncomplicated single-domain solution to this flow using an immersed solid treatment of the impeller and the LES-WALE model for simulation-based turbulence capturing (Nicoud and Ducros, 1999). This is a successor study to the previous 5L Eppendorf

New Brunswick STR study (Liovic et al., 2014); validation of the previous study and its role in the current study are discussed in the Results section.

Lagrangian particle tracking

The implementation of Lagrangian particle tracking here uses the standard conservation equations for translational and angular momentum to prescribe particle motion

$$\frac{d\mathbf{U}_p}{dt} = \frac{\mathbf{F}_p}{m_p} \quad (1)$$

$$\frac{d\hat{\omega}_p}{dt} = \frac{\mathbf{T}_p}{I_p} \quad (2)$$

The conservation equations, as well as the updates to the particle position and orientation, are solved using fourth-order Runge-Kutta time integration. Standard forces on particles from their motion in the fluid flow are included in the LPT solver:

$$\mathbf{F}_p = \mathbf{F}_p^{drag} + \mathbf{F}_p^{buoyancy} + \mathbf{F}_p^{VM} + \mathbf{F}_p^{Saffman} + \mathbf{F}_p^{Magnus} \quad (3)$$

where the superscripts denote the drag, buoyancy, virtual mass, Saffman and Magnus forces; Schiller-Naumann is used for the drag model. Standard expressions for the forces are used, and the contribution of the flow to particle torque is also included (Crowe et al. 1998).

CFD data mapping to LPT solver

For flow field-dependent forces such as the drag force, velocity data from the historical CFD database is interpolated. The database consists of flow fields of equal time spacing associated with spin-up and then fields associated with fully-developed STR operation. This decomposition into spin-up and fully-developed data is used to prescribe CFD flow field data over long-time LPT solver time integrations. In the current implementation of the virtual environment within which the LPT post-processor operates, cubic interpolation is used for temporal interpolation of flow field data at saved times during the course of the CFD run to the time instant in the LPT solver. At each saved time instant in the database, the unstructured-mesh data from the CFD database (ANSYS-CFX .csv files) is read in, nearest mesh nodes surrounding the Lagrangian particle in all octant directions are identified, and then inverse-distance interpolation is used to generate the fluid flow data for mapping to the particle.

Particle-particle and particle-wall interaction

The current LPT post-processor uses a hard sphere mode of particle-particle and particle-wall interactions, where the post-collision translational and angular velocities for generic particle-particle interaction outlined by Crowe et al. (1998) are used for both particle-particle and particle-wall interactions.

Infinite particle mass is used to locally represent the wall in a particle-wall interaction. The current implementation of the virtual environment linking the CFD database and the LPT solver reads in nodal data from the database and proceeds to reconstruct the geometry of the STR as a distance function level-set on a rectangular mesh in a stationary reference frame. In the course of LPT post-processor execution, close approach to the zero level of the distance function activates the particle-wall interaction module. Upgrading of the particle-wall interaction from a close approach to actual contact with the zero level then

results in a fictitious particle being temporarily generated and the particle-wall interaction being modelled in the same way as the particle-particle interaction.

RESULTS

Mobius 3L STR flow experimental visualisation

The importance of using LES-WALE in preference to more standard RANS-based technologies for capturing the vortical structure in transient STR flow was established in Liovic et al. (2012, 2014); quantitative validation against experiment was achieved in these studies because the STRs themselves were amenable to fluid flow measurement using Particle Image Velocimetry (PIV) because of their glass construction and smaller less intrusive sensors. The single-use Mobius 3L STR is not as amenable to PIV flow measurement because of its plastic construction and more internally intrusive sensors (temperature, DO, pH). The flow in the Mobius 3L STR was instead experimentally investigated using flow visualisation, in which the seeded STR flow was illuminated by a non-laser light source and filmed. Figure 1 shows an example snapshot of the particle distribution from the experiment. Particle streaks in the Figure indicate the presence of the more intense vortical structures; animation analysis was used to identify the location and directions of the circulation (shown in blue).

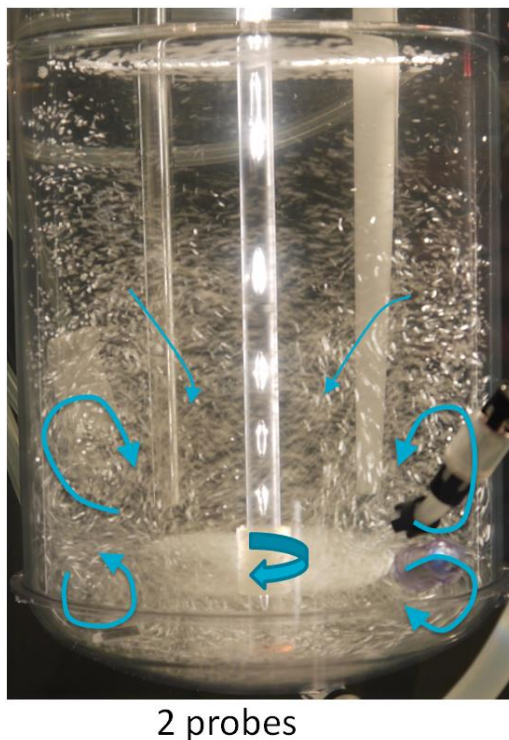


Figure 1: Local flow directions of vortical flow structures visible from video footage of Mobius 3L STR operation at 90 RPM, in the case of 2 probes being deployed.

An observation from previous experimental versus CFD comparisons of STR flows was that the vortical flow structures in velocity vector map animations of the WALE-based CFD results were generally slightly smaller than what was seen experimentally. One potential cause of such a discrepancy may arise from seeding particle inertia effects. The primary vortical structures driven by the

impeller are persistent, but away from these structures adjacent to the impeller the vortices are not as strong nor as persistent. Particles initially entrained into a strong vortex may break away from that vortex upon its weakening or disappearance. This enables particles to follow trajectories of lesser curvature; a number of such particle trajectories in the same general vicinity can take on the appearance of a flow structure that appears larger and more persistent than it actually is.

Mobius 3L STR flow CFD

Driving the flow in the 2.2 L of liquid bath in the Mobius 3 L STR at 90 RPM resulted in powerful radially outward ejection of flow from the impellers. Figure 2 is a representative instantaneous snapshot of the normalised velocity field extracted from the animation of all of the fields generated during the course of the simulation. Figure 2 indeed shows that the lower two sets of vortices (on the left side the lowermost counterclockwise vortex and the mid-level clockwise vortex (and mirrored on the right hand side)) has been established in the flow. Furthermore, the draft of fluid inwards and downwards shown by the uppermost arrows in Figure 1 indeed coincides with a downward draft in the CFD result in Figure 2 on the left hand side that seems to align with the outer boundary of a local clockwise circulation.

Figure 3 showing an instantaneous snapshot of the shear stress distribution highlights the power of the flow generated by the marine impeller rotating at 90 RPM. The $O(10^{-1})$ Pa shear stresses near the impeller are not representative of the rest of the liquid bath (in the $O(10^{-2}-10^{-3})$ Pa range). The time that microcarriers spend in the high-stress zone becomes important in linking the flow field to cell damage and cell fate, and will be considered later using the LPT post-processor. [Note that the LPT solver can also investigate the issue mentioned previously of reconciling experimental PIV data and CFD velocity vector map data: that will be done in future work in larger LPT computations.]

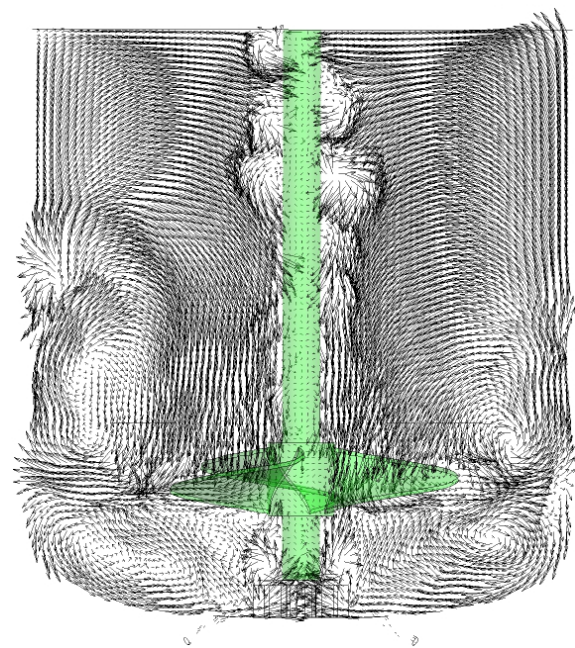


Figure 2: Sample instantaneous velocity vector map from single-fluid CFD model.

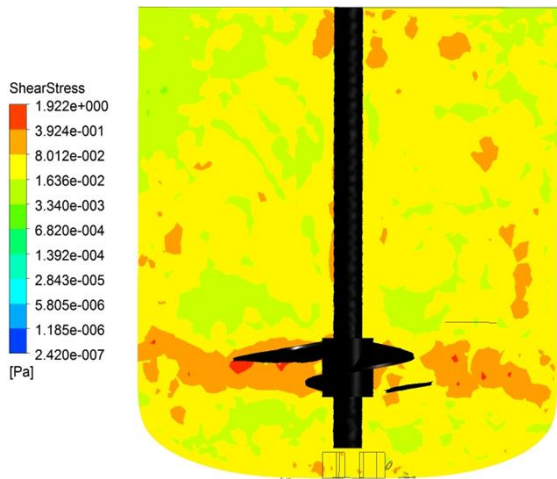


Figure 3: Sample instantaneous contour map of the shear stress magnitude in the vertical symmetry plane from single-fluid CFD model. [The shear stress includes modelled subgrid-scale shear stress contributions.]

Particle suspension

For the studies of particle suspension and shear stress exposures in the STR, the liquid bath in the first instance is presumed to feature a low solid concentration hence enabling particle-particle collision to be ignored for now. Figure 4 shows the trajectories of 50 particles after 10 seconds for the case of $\rho_P = 1045 \text{ kg/m}^3$, which shows most of the particles have not penetrated the jet flow of the impeller as yet. From an initial settled state, Figure 4 and Figure 5(a) suggest that the approximately 20 percent of particles that do penetrate the jet flow and rise up into the upper reaches of the liquid bath were well positioned to be entrained by the lowermost vortices early in the spin-up process. When heavier microcarriers are used, penetration of microcarriers into the upper reaches of the liquid bath is largely suppressed.

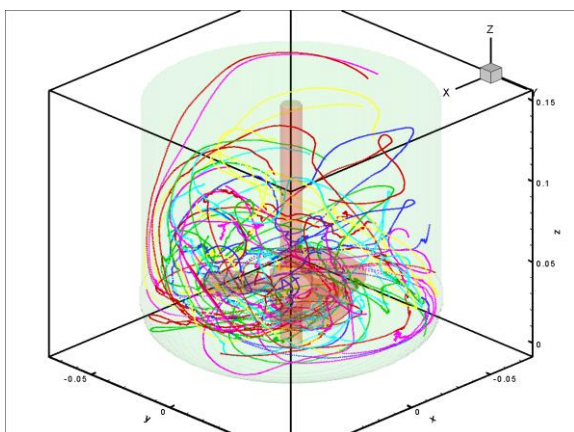


Figure 4: Lagrangian particle trajectories at $t=10 \text{ s}$ of STR operation, for the case of $\rho_P = 1045 \text{ kg/m}^3$.

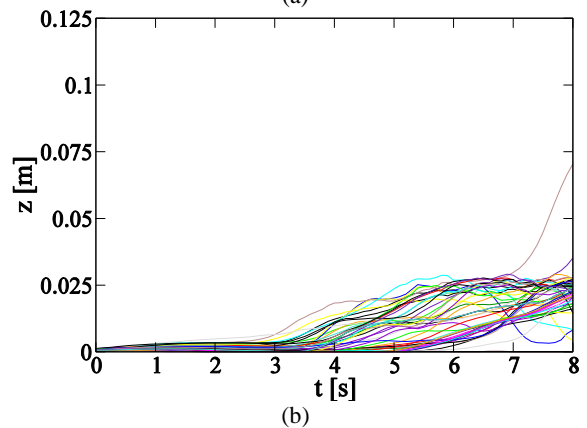
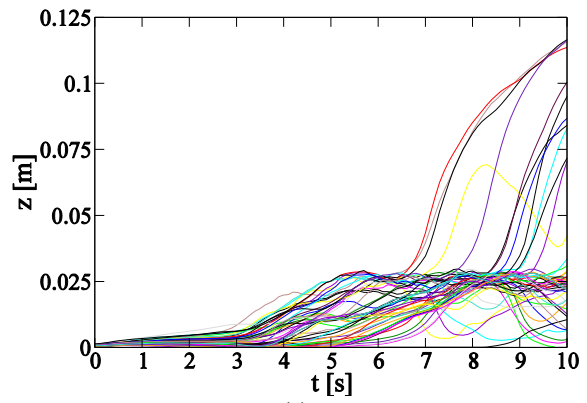


Figure 5: Elevation of particles during the course of spin-up: (a) $\rho_P = 1045 \text{ kg/m}^3$ and (b) $\rho_P = 1070 \text{ kg/m}^3$.

Shear stress exposures

The process of microcarrier suspension is shown in Figure 6 to be accompanied by distinct phases of shear stress exposure. Initial particle suspension involves an imparting of $O(10^{-3}) \text{ Pa}$ shear stresses, before a gradual rise in stress levels as the microcarriers rise towards the sweep path of the impeller. Once in the sweep path, the microcarriers are subjected to higher fluctuating stresses. Even though the stresses are fluctuating, the stress levels in the impeller sweep path are generally above 0.01 Pa . This level, combined with the power of the ejected jet at 90 RPM impeller speed, provides little confidence that the microcarriers are not being exposed to high stress levels associated with cell damage, changes in cell fate and undesirable lineage commitment. Some stress histories late on in the history experience sharp drops in stress levels, which is indicative of stress levels higher up in the liquid bath. Further LPT solver studies with longer time durations will seek to identify what constitutes a short time exposure to a high stress level by a stem cell, and whether brevity of exposure to the high-stress zone ameliorate tendencies for cell damage and changes in fate.

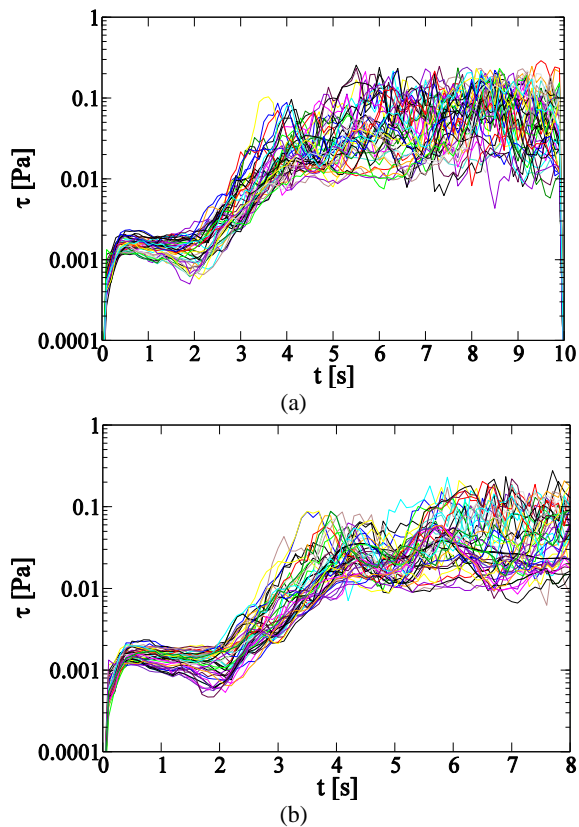


Figure 6: Particle shear stress exposures during the course of spin-up: (a) $\rho_p = 1045 \text{ kg/m}^3$ and (b) $\rho_p = 1070 \text{ kg/m}^3$.

CONCLUSION

This paper presents a Lagrangian particle tracking (LPT) solver and investigates some of the potential limitations associated with the reduced coupling between the particle and fluid flow solutions, before demonstrating the utility of the LPT post-processor as a component of a virtual environment for bioreactor analysis. Prior to that, the CFD computation of the STR flow was shown to give realistic results and hence form the ideal basis for the CFD database. The LPT solver run in this work identified expected effects of particle density in the suspension. The utility of this approach is already proving beneficial, in that microcarrier properties and seeding of stem cell bioreactors are already being studied without need for repeated CFD simulations; investigations that would otherwise take weeks of fully coupled CFD+LPT can now be done in a few days, and without the charge for usage of parallel clusters.

ACKNOWLEDGEMENTS

Seed funding for this project was provided by the CSIRO Intelligent Processing Future Science Platform (IP-FSP). Additional support was provided through CSIRO Mineral Resources.

REFERENCES

- BERRY, J.D., GODARA, P., LIOVIC, P. and HAYLOCK, D.N. (2015), "Predictions for optimal mitigation of paracrine inhibitory signalling in haemopoietic stem cell cultures", *Stem Cell Res. Ther.*, **6**, 58.
- CROUGHAN, M.S., HAMEL, J.-F. and WANG, D.I.C. (1987), "Hydrodynamic effects on animal cells grown in microcarrier cultures", *Biotechnol..Bioeng.*, **29**, 130.
- CROWE, C., SOMMERFELD, M. and TSUJI Y., (1998), "Multiphase Flows with Droplets and Particles", CRC Press.
- LIOVIC, P., ŠUTALO, I.D., MEAGHER, L. and LOVREČIĆ, G.O., (2014), "Computations of flow environments in medium-scale stirred-tank bioreactors for stem cell expansion", *Proc. ASME FEDSM-2014*, ASME, Chicago, IL, USA, August 3-7.
- LIOVIC, P., ŠUTALO, I.D., STEWART, R.L., GLATTAUER, V. and MEAGHER, L. (2012), "Characterisation of fluid stresses and microcarrier dynamics in a stirred bioreactor", *Proc. 9th Int. Conf. CFD Min. Proc. Ind.*, CSIRO, Melbourne, Australia, Dec. 9-11.
- MILLIPORE, (2013), "Scale-up of human mesenchymal stem cells on microcarriers in suspension in single-use bioreactor", *Technical Brief*, EMD Millipore.
- NICOUD, F. and DUCROS F., (1999), "Subgrid-scale stress modelling based on the square of the velocity gradient tensor", *Flow Turbul. Combust.*, **62**, 183-200.
- OLMER, R., KROPP, C., HUETHER-FRANKEN, C. and ZWEIGERDT, R., (2013), "Scalable expansion of human pluripotent stem cells in Eppendorf BioBLU® 0.3 single-use bioreactors", *Application Note*, Eppendorf.
- PARK, J.Y., YOO, S.J., PATEL, L., LEE, S.H. and LEE, S.-H., (2010), "Cell morphological response to low shear stress in a two-dimensional culture microsystem with magnitudes comparable to interstitial shear stress", *Biorheology*, **47**, 165-178.
- ZHAO, F., CHELLA, R. and MA, T. (2007), "Effects of shear stress on 3-D human mesenchymal stem cell construct development in a perfusion bioreactor system: experiments and hydrodynamic modeling", *Biotechnol..Bioeng.*, **96**, 584-595.